

## **MICROSTRUCTURE AND MECHANICAL PROPERTIES OF AlSi10Mg PERMANENT MOULD AND HIGH PRESSURE VACUUM DIE CASTINGS**

Z. Zhang <sup>1,\*</sup>, M.-Y. Liu <sup>1</sup>, F. Breton <sup>2</sup>, and X.-G. Chen <sup>1</sup>

<sup>1</sup> *Department of applied sciences, University of Quebec at Chicoutimi,  
Saguenay, (Quebec), Canada, G7H 2B1*

(\*Corresponding author: zhan\_zhang@uqac.ca)

<sup>2</sup> *Arvida Research and Development Centre, Rio Tinto,  
Saguenay (QC), Canada, G7S 4K8*

### **ABSTRACT**

The microstructures of AlSi10Mg foundry alloy in permanent mould (PM) and high pressure vacuum die (HPVD) castings were analyzed and compared. The as-cast microstructures of two castings mainly consisted of eutectic silicon particles, primary Mg<sub>2</sub>Si and Fe-rich intermetallic phases. The surface layer in HPVD castings, which has a unique feature and different structures, was carefully characterized. The dimension variation of microstructural phases along the cross section in PM samples is less than that in HPVD samples, although the size of microstructural phases in PM samples was much larger than that in HPVD samples. The mechanical properties of PM and HPVD samples were evaluated on as-cast and T6-treated conditions. The tensile properties of HPVD castings are remarkable better than those of PM castings on the as-cast condition. The T6 heat treatment greatly improves the tensile strength of PM castings while it has limited impact on the tensile strength of HPVD castings.

### **KEYWORDS**

AlSi10Mg foundry alloy, Permanent mould casting, High pressure vacuum die casting, Microstructure, Mechanical properties

## INTRODUCTION

The AlSi10Mg alloys are widely applied to the high pressure die casting (HPD) and high pressure vacuum die casting (HPVD). In the HPD process, the melt is injected into the die cavity under a high speed (30–50 m/s in the gate velocity for aluminum alloys), and solidified under a high pressure (up to 200 MPa in the cavity) and with a high cooling rate (up to  $\sim 10^3 \text{ Ks}^{-1}$ ) (Gourlay, Laukli & Dahle, 2007; Ji, Wang, Watson & Fan, 2013). This results in a unique microstructure feature that is different to other casting processes under gravity. One major concern in HPD castings is porosity due to trapped air in the cavity (Ji et al., 2013), which seriously restricts the application of a heat treatment on the improvement of mechanical prosperities because of the formation of blisters on casting surfaces. For the process improvement, the high pressure vacuum die casting was developed in 1980s (Uchida, 2009). In this process, the melt is injected into the die cavity under reduced pressure (vacuum), which greatly reduces gas porosity in castings due to effectively avoiding the trapped air. Consequently, HPVD castings are heat-treatable without the formation of blisters on castings surface during heat treatment. The HPVD process has been widely applied to produce high quality structural castings in recent years attributed to reliable vacuum system development (Uchida, 2009). However, the microstructure features of HPVD castings are not systemically characterized yet.

On the other hand, in the permanent mould casting (PM), the melt fills the mould cavity under gravity with a low speed ( $< 1.5 \text{ m/s}$  in the gate for aluminum alloys) and solidifies at low cooling rate ( $< 10 \text{ Ks}^{-1}$  for aluminum alloys) (Wang, Zheng, Qu, Zhou & Xu, 1984; Hamasaiid et al., 2007). Generally, there is much less gas porosity and no special surface layer in PM castings. Their mechanical properties can be greatly improved through appropriate heat treatment, such as T6 heat treatment.

The aim of the present work is on quantitative characterization of the microstructure of both PM and HPVD castings to understand the effect of casting processes on the microstructure and mechanical properties. Moreover, the mechanical properties on as-cast and T6-treated conditions of both castings were evaluated to reveal the correlation between heat treatments and mechanical properties.

## EXPERIMENTAL

For the permanent mold casting, the AlSi10Mg alloy was prepared with commercially pure Al (99.7%), pure Mg (99.9%), Al-25%Mn, Al-25%Fe, and Al-50%Si master alloys. For each batch, approximately 3 kg of materials were melted in an electrical resistance furnace. The melt was kept at 720–750°C for 30 min and degassed for 15 min, and then poured into a permanent copper mold preheated at 250°C. The dimension of the cast plates is 100 mm  $\times$  80 mm with a thickness of 4 mm. The HPVD castings were produced by a cold chamber vacuum die casting machine, provided by Rio Tinto Aluminum. The dimension of the cast plates is 220 mm  $\times$  65 mm with a thickness of 2.5 mm. The chemical compositions of two castings analyzed by an optical emission spectrometer are listed in Table 1, which are very similar. The T6 heat treatment was carried out with the solution treatment at 500°C for 1 h followed by the aging at 170°C for 2.5 h.

Table 1. Chemical compositions of experimental alloys (wt.%)

Castings	Si	Mn	Mg	Ti	Sr	Fe	Al
PM	10.10	0.55	0.59	0.08	0.012	0.20	bal.
HPVD	10.10	0.55	0.55	0.08	0.011	0.18	bal.

Conventional metallographic polishing was applied for the sample preparation. An optical microscope with an image analyzer (CLEMEX software PE4-0) was used for observation and quantitative characterization of the microstructural variables, such as the equivalent diameter, aspect ratio, volume fraction, distribution of various phases. A scanning electron microscope (SEM, JSM-6840LV) equipped with an energy dispersive spectrometer (EDS) was employed to observe and characterize different types of phases. The microstructure variables in five zones along the sample cross section were analyzed with image analysis. In each zone, eight optical images (500x) were quantitatively analyzed.

Vickers hardness measurements were performed using a hardness test machine (Nextgen NG-1000CCD) with a load of 100 g and 15 s dwell period on the polished surface following the ASTM E92. The average value and standard deviation were reported from a minimum of 10 measurements. The tensile tests were carried out at room temperature using an Instron universal testing machine according to the ASTM B557. Sub-size tensile test bars (100 mm in the overall length and 25 mm in the gage length) were used. The tensile properties, namely the ultimate tensile strength (UTS), yield strength (YS) at a 0.2% offset strain and fracture elongation (El), were reported as an average value of four test bars. The electrical conductivity was measured by Sigmascope SMP10 unit. Five measurements were conducted for each sample.

## RESULTS AND DISCUSSION

### Microstructure of HPVD and PM Samples

Figure 1 shows the optical and SEM images of the HPVD microstructure. Under optical microscopy, the rosette-like aluminum grains present with a light color, Al-Si eutectic is grey color and primary  $Mg_2Si$  particles show dark color (Figure 1(a) and (b)). The Fe-rich intermetallic phase can be better observed under SEM backscattered images (Figure 1(c) and (d)), which are the dot- and block-like particles with white color. The surface layer in HPVD castings has a unique feature and consists of 1) a skin sublayer, 2) a eutectic-rich sublayer and 3) an aluminum grain-rich sublayer, as indicated in Figure 1(a). The skin sublayer is directly adjacent to the sample surface with 60–100  $\mu m$  in thickness, in which the size of aluminum grains and silicon particles is much smaller than that in the center position (Figure 1(b)). Next to the skin sublayer, it is a eutectic-rich sublayer, in which the fraction of Al-Si eutectic is much more than the other positions of the sample. Adjacent to the eutectic-rich sublayer, there is an aluminum grain-rich sublayer. After the surface layer (approximately 180–200  $\mu m$ ) towards the center, the microstructure becomes uniform as shown in Figure 1(b). In a particle suspension system, fluid flow affects the particle distribution (Ferguson & Kembrowski, 1991). In the HPVD die cavity filling process, the melt flow contains many aluminum grains, which are at first solidified in a shot chamber or on the die wall, and some of the aluminum grains would then dropped off from the wall under the melt flow action. The skin sublayer forms on die cavity wall when the melt enters the cavity from a gate due to the high cooling rate on the wall. A shear force arises between the solidified skin sublayer on die cavity wall and the melt flow. Under the shear force, solute-rich liquid aluminum is concentrated on the interfaces (solidified skin sublayer/melt) to reduce the flow resistance, and the aluminum particles/grains are pushed to one side. Consequently, this results in the formation of a eutectic-rich sublayer and an aluminum grain-rich sublayer.

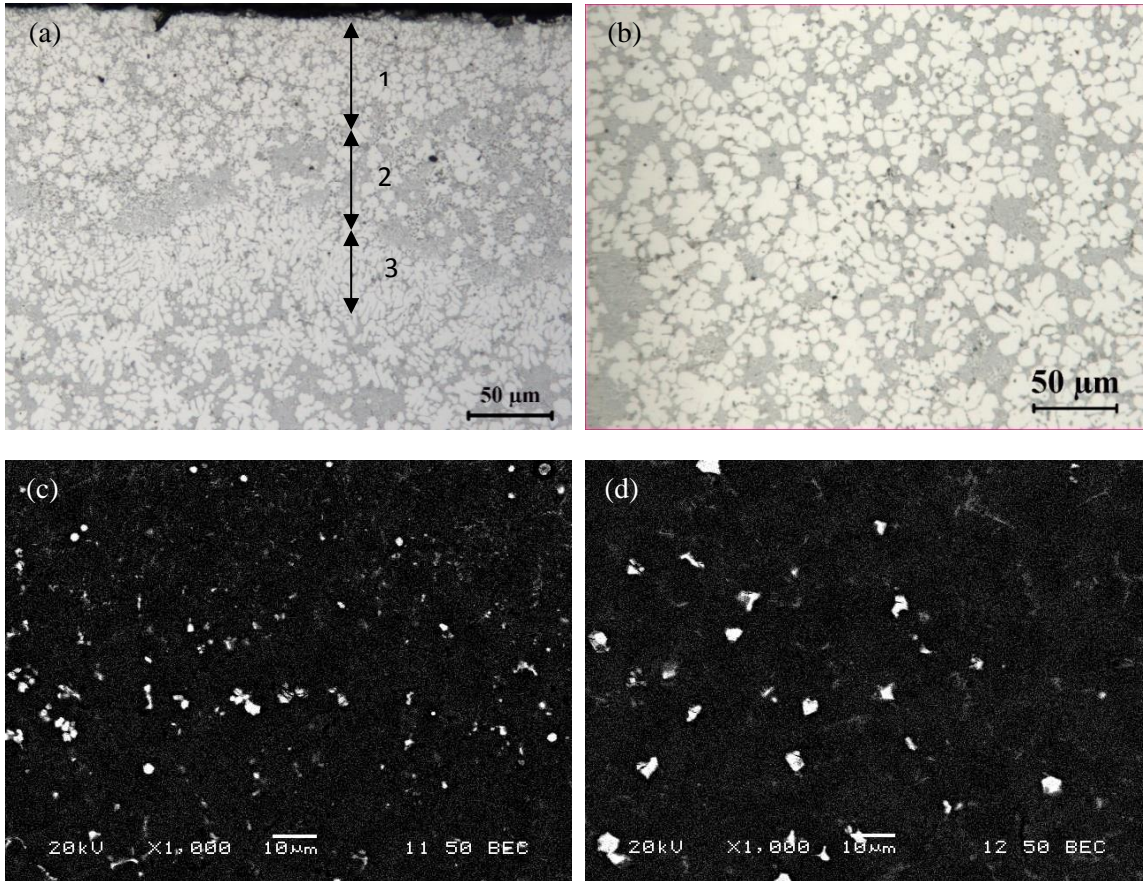


Figure 1. Microstructure of the as-cast HPVD sample: optical images near cast surface (a) and at the center (b); SEM electron backscattered images near cast surface (c) and at the center (d).

The quantitative image analysis results of the HPVD microstructure are shown in Figure 2. The secondary dendrite arm spacing (SDAS) and aluminum grain size vary from the cast surface to the center (Figure 2(a)). The average value of SDAS in the skin sublayer (2.5  $\mu\text{m}$ ) is much smaller than that at the center (6  $\mu\text{m}$ ). The aluminum grains size varies along the cross section of the HPVD sample (Figure 2 (a)) and increases from the cast surface toward the center. The equivalent diameter of the aluminum grains in the skin sublayer (4.2  $\mu\text{m}$ ) is approximately 60% of that in the center (7.2  $\mu\text{m}$ ). The similar phenomenon is observed on the eutectic Si and primary  $\text{Mg}_2\text{Si}$  particles as well as Fe-rich intermetallic particles, i.e. the sizes of those phases increase with the increasing of the distance from the cast surface to the center (Figure 2(b), (c) and (d)).

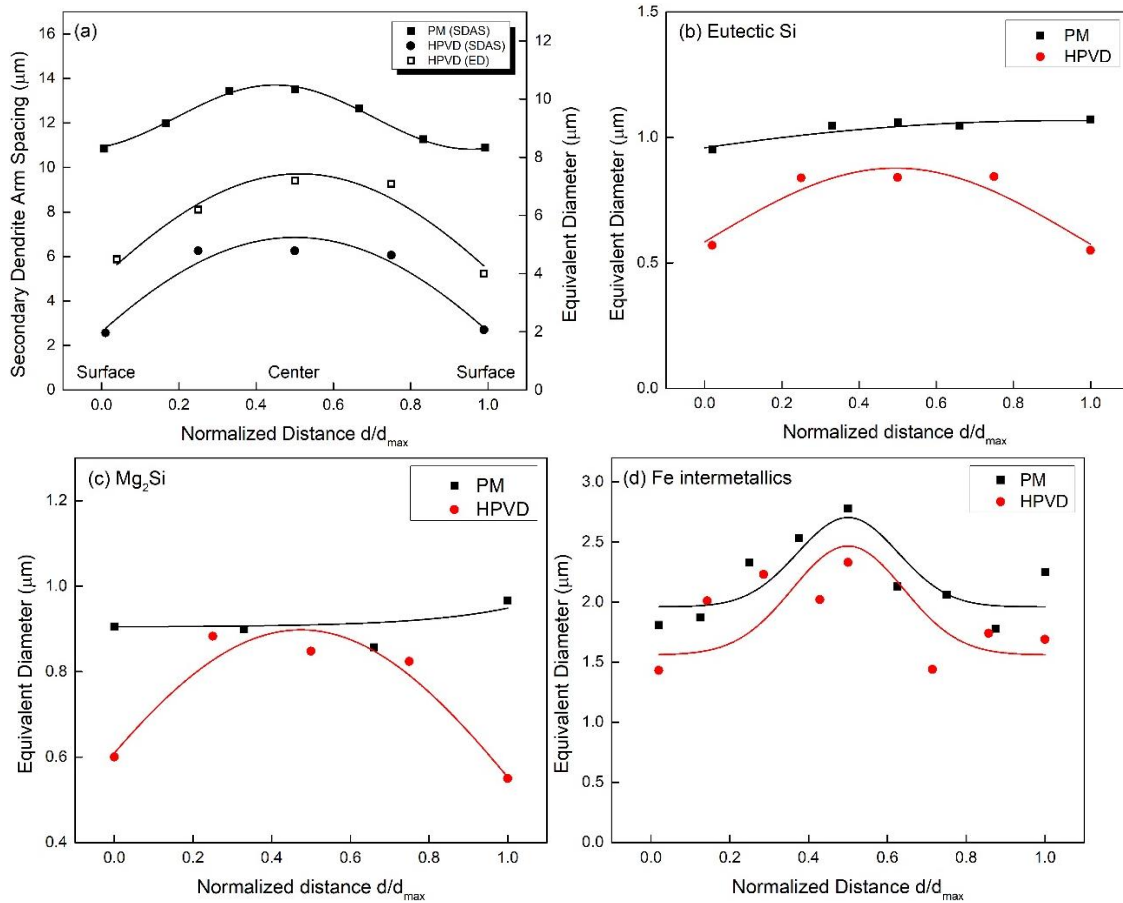


Figure 2. The secondary dendrite arm spacing (SDAS) and equivalent diameter of aluminum grains (a); the equivalent diameter of Si (b), primary  $\text{Mg}_2\text{Si}$  (c) and Fe-rich intermetallics (d) along the cross section of PM and HPVD samples.  $d$ : the distance from one edge to other;  $d_{max}$ : the sample thickness.

The microstructure of the PM sample near cast surface and at the center is shown in Figure 3, which is composed of aluminum dendrite cells, Al-Si eutectic, primary  $\text{Mg}_2\text{Si}$  and Fe-rich intermetallic particles. The Fe-rich intermetallic particles have block shape near cast surface (Figure 3(c)) and the long needle-like morphology at the center (Figure 3(d)). The types of the phases in PM samples are the same as those in HPVD samples. However, the morphology and size of those phases are greatly different in the two castings. The SDAS in the PM sample increases from the cast surface to the center but it is obviously larger than that in the HPVD sample (Figure 2(a)) due to a low cooling rate of PM casting. However, the SDAS variation of PM sample (from  $8.2 \mu\text{m}$  at the surface to  $10.5 \mu\text{m}$  in the center) is smaller than that of the HPVD sample (from  $4 \mu\text{m}$  at the surface to  $7 \mu\text{m}$  at the center). In general, the size of eutectic Si and primary  $\text{Mg}_2\text{Si}$  in the PM sample is greater than that in the HPVD sample (Figure 2(b) and (c)). In addition, the size of eutectic Si and primary  $\text{Mg}_2\text{Si}$  almost does not vary along the PM sample cross section. Although the size of Fe-rich intermetallics in both PM and HPVD samples increases from the cast surface to the center, the average size of Fe-rich intermetallics in the PM sample is much larger than that in the HPVD sample (Figure 3(d) vs Figure 1(d)).

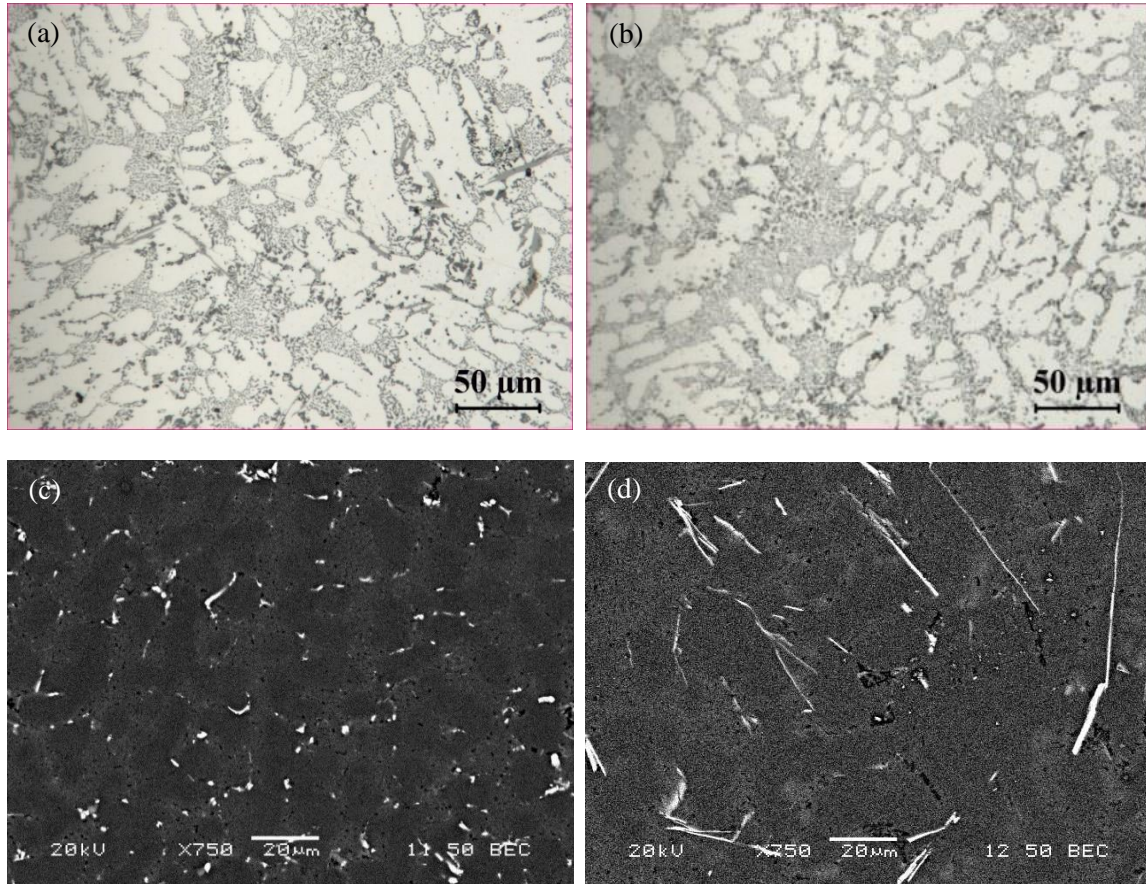


Figure 3. Microstructure of as-cast PM samples: optical images near cast surface (a) and at the center (b); SEM electron backscattered image near cast surface (c) and at the center (d).

The Si and Mg distributions along the sample cross section in both HPVD and PM castings were investigated by EDS-SEM as shown in Figure 4. Each analysed data in Figure 4 was the average value of Si and Mg concentration in a measured area in which there were around five to ten aluminum grains or dendrite cells shown in Figs. 1(a) & (b) and 3(a) & (b). The Si content in the surface layer of the HPVD sample (within 200-220  $\mu\text{m}$ ) varies remarkably (Figure 4(a)). In the skin sublayer, the Si content is lower than the average Si content (10.1%) in the alloy, whereas the Si in the eutectic-rich sublayer is much higher than that in the skin sublayer, followed a dramatic decrease in the Si content in the aluminum grain-rich sublayer. After the three sublayers, the Si content fluctuates between 10-11% in the distance from 0.3 mm to 1.0 mm. Further toward the sample center, the Si content decreases again. This indicates that there exists a macrosegregation of Si in the HPVD sample. Moreover, the Mg macrosegregation was also observed (Figure 4(b)). The Mg concentration in the cast surface (0-220  $\mu\text{m}$ ) is much higher than the average Mg content (0.55%) in the middle of the sample. After 1.0 mm, the Mg concentration decreases considerably toward the center. The macrosegregation of Si and Mg is attributed to the inverse segregation and exudation during the solidification under high pressure (Gourlay et al., 2007; Flemings, 1974). On the other hand, there is no significant macrosegregation of Si and Mg in the PM sample. The Si content in the PM sample is fluctuated between 9-11% (Figure 4(c)) and Mg varies between 0.48% and 0.72% along the cross section (Figure 4(d)).

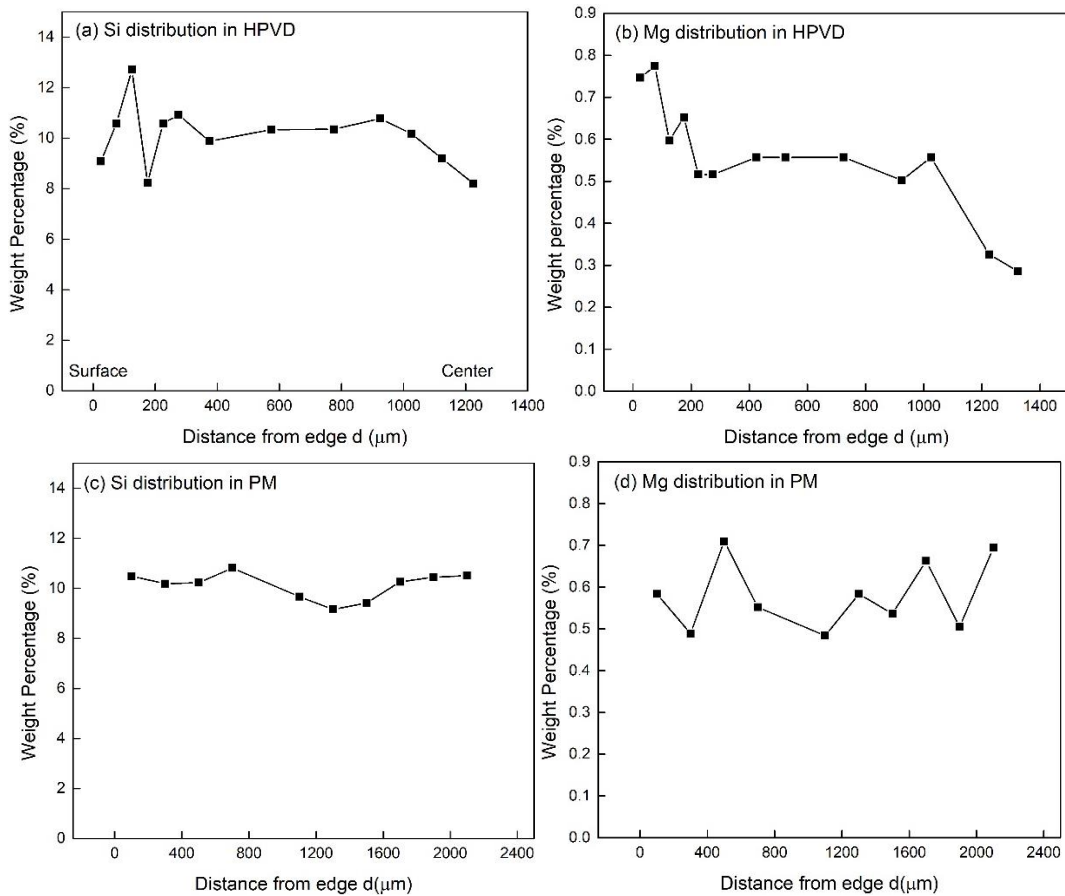


Figure 4. Si (a) Mg (b) distribution in the HPVD sample; Si (c) Mg (d) distribution in the PM sample.

Based on the quantitative image analysis results, it is interesting to find that the area fraction of primary  $Mg_2Si$  in the PM samples are four times higher than that in HPVD samples (0.21 vol.% in PM vs 0.05 vol.% in HPVD), although the Mg contents are similar in both samples (0.59 in PM and 0.55% in HPVD, see in Table 1). The measured electrical conductivity (EC) shows that the EC of PM samples is 34.35 %IACS but it is 29.87 %IACS in HPVD samples on as-cast condition. This indicates that there are more solute Si and Mg supersaturated in the aluminum matrix of HPVD samples than that in PM samples.

Figure 5 shows the microstructure of HPVD and PM samples after T6 heat treatment. The plate-like eutectic Si on as-cast condition becomes more spherical after the T6 treatment in both samples (Figure 5(a) and (b)). However, the size and morphology of the Fe-rich intermetallics in HPVD and PM samples does not change after T6 treatment. They are still dot- or rod-like morphology in the HPVD sample (Figure 5(c)) and the long needle-like shape in the PM sample (Figure 5(d)).

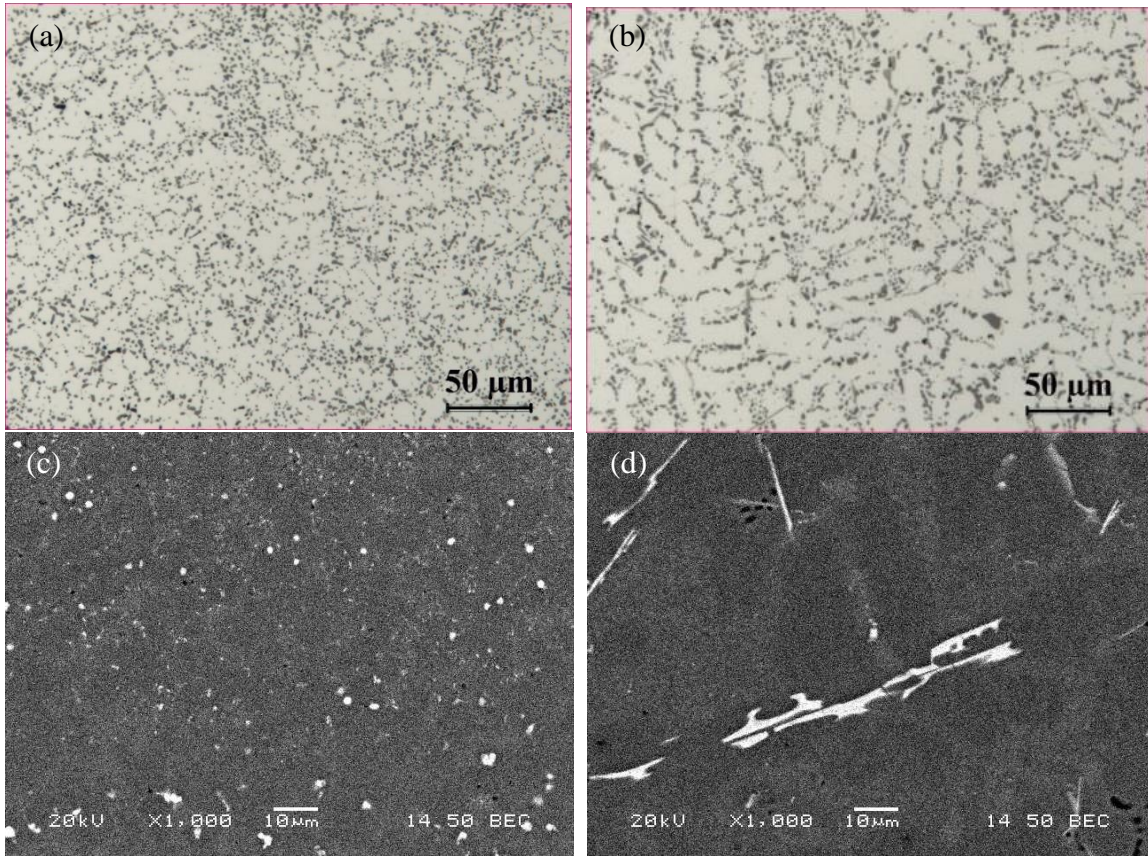


Figure 5. Microstructure in the sample center after T6 heat treated: optical images of HPVD (a) and PM (b) samples; SEM backscattered electron image of HPVD (c) and PM (d) samples.

### **Mechanical Properties on As-Cast Condition and After T6 Heat Treatment**

Figure 6(a) shows the hardness profile along the cross section of HPVD and PM samples on the as-cast condition. The hardness near cast surface is considerably higher than that in the middle of the HPVD sample. For example, the hardness is ~100 HV near cast surface but it is ~90 HV in the middle part of the sample. In the region near cast surface, the concentration of Si and Mg is higher than that in the middle part in the HPVD sample due to the macrosegregation (Figure 4). The high hardness in the region near cast surface is mostly attributed to the solid solution strengthening. On the other hand, the hardness fluctuates between 85 HV to 88 HV along the cross section of the PM sample. The hardness variation along the cross section of the PM sample is small. The average hardness in the middle part of the HPVD sample is slightly higher than that in the PM sample.

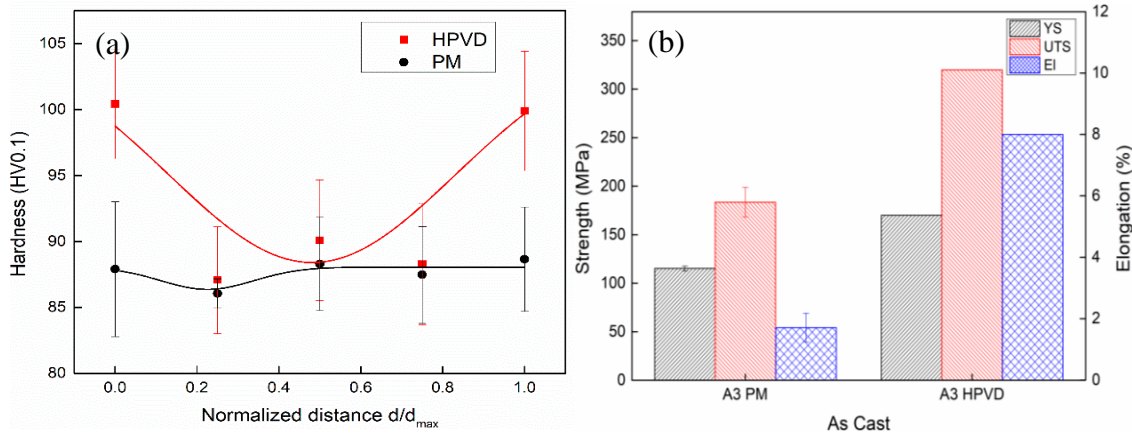


Figure 6. Mechanical properties of HPV and PM samples on as-cast condition: the hardness profile along the cross section (a), and the tensile properties (b). Tensile properties of HPV are taken from (Breton & Fourmann, 2016).  $d$ : the distance from one edge to other;  $d_{max}$ : the sample thickness.

The tensile properties of HPV (Breton & Fourmann, 2016) and PM samples on the as-cast condition are shown in Figure 6(b). It is evident that the tensile properties of HPV castings are remarkable better than those of PM castings. The YS of the PM sample is approximately 68% of that of the HPV sample while the UTS of the former is approximately 57% of that of the latter. Particularly, the elongation of the PM casting is quite low and only 21% of that of the HPV casting, which is most likely related to the long needle-like Fe-rich intermetallics in the PM casting.

Figure 7(a) shows the hardness profile along the cross section of HPV and PM samples after T6 heat treatment. The hardness near the cast surface of two castings is slightly higher than that at the sample center. The hardness of the HPV sample varies between 112 HV and 117 HV. Compared to the as-cast condition, the hardness difference between the surface and center after T6 is smaller, which would be attributed to the disappearance of solute supersaturation at the near surface region. On the other hand, the hardness of the PM sample varies between 117 HV and 121 HV. It is interesting to note that the hardness of the PM sample is higher than that of HPV samples on the T6 condition. The hardness increases in PM and HPV samples are 38% and 24% respectively, relative to the hardness on the as-cast condition. In other words, the effect of the T6 treatment on the hardness improvement is more predominant in the PM sample.

Figure 7(b) shows the tensile results of HPV (Breton & Fourmann, 2016) and PM samples on the T6 condition. For HPV castings, the YS after T6 reaches 175 MPa, which is an approximate 3% increase over the as-cast condition. The UTS is only 257 MPa, which is an approximate 20% decrease compared to the as-cast condition. The elongation of the HPV sample increases from 8% on as-cast condition to 10% after T6. It seems that the T6 treatment can only improve the elongation of HPV castings, but it has limited impact on the tensile strength. For PM castings, the YS and UTS reach 183 MPa and 247 MPa respectively, which present a 59% increase in YS and a 35% increase in UTS over that on the as-cast condition. It is evident that the T6 treatment greatly improves the tensile strength of PM castings. After T6 heat treatment, the tensile strength of PM castings can reach the similar level of HPV castings. However, the elongation of PM castings is always much lower than that of HPV castings on both as-cast and T6 conditions.

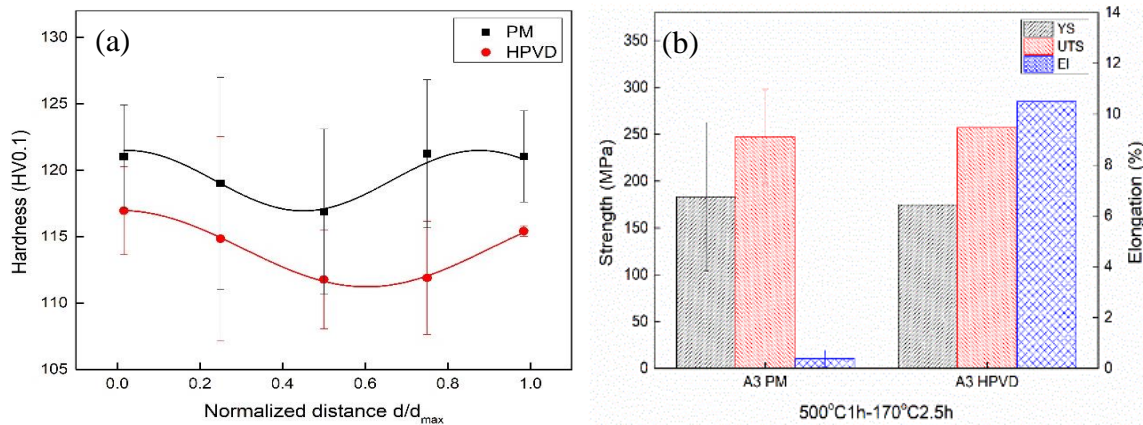


Figure 7. Mechanical properties of HPVD and PM samples on T6-treated condition: the hardness profile along the cross section (a), and the tensile properties (b). Tensile properties of HPVD are taken from (Breton and Fourmann, 2016).  $d$ : the distance from one edge to other;  $d_{max}$ : the sample thickness.

## CONCLUSIONS

- (1) In the high pressure vacuum die (HPVD) casting, there exists a surface layer that has a unique feature and different structures. The surface layer can be divided into 1) a skin sublayer directly adjacent to the cast surface, 2) a eutectic-rich sublayer next to the skin sublayer and followed by 3) an aluminum grain-rich sublayer.
- (2) The macrosegregation of Si and Mg in the cross section of as-cast HPVD samples has been observed. In general, the Si and Mg concentrations are enriched in the surface layer and depleted in the center of the sample. On the other hand, there is no significant macrosegregation of Si and Mg in the permanent mold (PM) samples.
- (3) The microstructure of PM samples is composed of the same phases as those of HPVD samples. The dimension variation of microstructural phases along the cross section in PM samples is less than that in HPVD samples, although the size of microstructural phases in PM samples is much larger than that in HPVD samples.
- (4) The hardness near the cast surface is considerably higher than that in the middle of as-cast HPVD samples. The hardness in the middle part of the HPVD sample is slightly higher than that in the PM sample on the as-cast condition. However, after T6 heat treatment the hardness of the HPVD sample is lower than that of the PM sample.
- (5) The tensile properties of HPVD castings are remarkable better than those of PM castings on the as-cast condition. The T6 heat treatment greatly improves the tensile strength of PM castings while it has limited impact on the tensile strength of HPVD castings. After T6 treatment, the tensile strength of PM castings can reach the similar level of HPVD castings.

## ACKNOWLEDGMENTS

The authors would like to acknowledge the financial support of the Natural Sciences and Engineering Research Council of Canada (NSERC) and Rio Tinto Aluminum through the NSERC Industry Research Chair in the Metallurgy of Aluminum Transformation at University of Quebec at Chicoutimi.

## REFERENCES

- Breton, F., & Fourmann, J. (2016). Alloys with high strength and ductility for high pressure vacuum die casting in automotive body structure applications: impact of heat treatment on mechanical properties. *Die casting congress & tabletop, Columbus, OH, USA*.
- Ferguson, J., & Kemblowski, Z. (1991). *Applied fluid rheology*. Springer.
- Flemings, M. C. (1974). *Solidification processing*. Wiley - VCH Verlag GmbH & Co. KGaA.
- Gourlay, C. M., Laukli, H. I., & Dahle, A. K. (2007). Defect band characteristics in Mg-Al and Al-Si high-pressure die castings. *Metallurgical and Materials Transactions A*, 38(8), 1833-1844.
- Hamasaiid, A., Dargusch, M. S., Davidson, C. J., Tovar, S., Loulou, T., Rezai-Aria, F., & Dour, G. (2007). Effect of mold coating materials and thickness on heat transfer in permanent mold casting of aluminum alloys. *Metallurgical and materials Transactions A*, 38(6), 1303-1316.
- Ji, S., Wang, Y., Watson, D., & Fan, Z. (2013). Microstructural evolution and solidification behavior of Al-Mg-Si alloy in high-pressure die casting. *Metallurgical and Materials Transactions A*, 44(7), 3185-3197.
- Uchida, M. (2009). Development of vacuum die-casting process. *China Foundry*, 6(2), 137-144.
- Wang, L.-Y., Zheng, L.-S., Qu, W.-T., Zhou, X.-C., & Xu, J.-W. (1984) p.196. Special casting processes. *Industry Press, Beijing, China*.